Global DIC algorithm for vibrating and rotating object tracking

Global DIC algorithm for vibrating and rotating object tracking

Journal of Physics: Conference Series **3179** (2026) 012010 doi:10.1088/1742-6596/3179/1/012010

Global DIC algorithm for vibrating and rotating object tracking

P. Neri*[1, [0000-0003-0730-0893]], A. Paoli[1,[0000-0002-1918-3033]], S. Occhipinti[2,[0000-0003-2792-795X]], A. Cesaretti[2,[0009-0003-3320-7905]], D. Botto[2,[0000-0002-0557-7162]] and C.M. Firrone[2,[0000-0002-1817-7686]]

[1]Department of Civil and Industrial Engineering, University of Pisa, Pisa Italy
[2]Department of Mechanical and Aerospace Engineering, Politecnico di Torino, Turin, Italy

*E-mail: paolo.neri@unipi.it

Abstract. Digital Image Correlation (DIC) is a widely used non-contact method for full-field displacement measurement under static and dynamic conditions. However, conventional algorithms struggle with large rotations, typically limited to 10–15°, making them unsuitable for rotating objects like wheels, turbines, or gears. Current workarounds involve using databases of static images at various angles to find a suitable reference image, but this approach lacks flexibility. This research presents a global DIC algorithm capable of tracking rotating objects without relying on image databases. A grid of points is defined on the reference image and numerically rotated around a specified center. Bicubic spline interpolation is used to estimate grey levels at non-integer positions in the deformed image. These are compared with reference values to compute an error, minimized through an optimization process based on a Gauss-Newton scheme. The method was validated on experimental images of a rotating PC fan, showing effective tracking for angles up to 90°.

1. Introduction

In rotor dynamics, it is essential to accurately characterize the dependence of modal parameters, such as natural frequencies and damping ratios, on rotational speed. Variations in modal parameters primarily arise from gyroscopic effects and centrifugal stiffening. As the rotational speed approaches the critical speed of the structure, the risk of resonance-induced failures increases markedly, underscoring the importance of accounting for dynamic effects in the design process. Traditionally, strain gauges have been the primary tool for monitoring rotor vibrations due to their reliability and direct strain measurement. However, their use presents several challenges: they require complex data transmission solutions (e.g., slip rings), can alter system dynamics through added mass, have limited operational life, and only provide localized measurements. These limitations have led to a growing interest in non-contact measurement techniques. Scanning Laser Doppler Vibrometers (SLDV), when combined with optical derotators, offer high-resolution pointwise vibration measurements without physical contact. The optical derotator allows the laser beam to follow the rigid rotation of the disk by employing a controlled optical rotation unit synchronized with the rotor's speed. This setup provides a non-invasive, accurate device to capture vibration data. However, the high cost of commercial systems remains a barrier. Cost-effective alternatives have been explored, such as a custom-built derotator paired with an SLDV for fan vibration analysis [1], or mirror-based tracking systems using LDVs [2]. Despite their lower cost, these methods are highly sensitive to misalignment and offer limited

spatial resolution. Blade Tip Timing (BTT) has emerged as a measurement technique for rotating bladed disks. By recording the time of arrival of blade tips through fixed sensors, BTT enables monitoring of blade tip displacements during rotation. While in most conventional configurations the sensors are positioned radially inward [3], different probe configurations have been explored to measure other displacement components [4]. Even if effective, BTT remains inherently one-dimensional and is confined to discrete measurement points at the blade tips. On the other hand, recent advancements in video-based techniques have opened new avenues for dynamic rotor analysis. Stereophotogrammetry, for example, has been used to monitor three-dimensional deformation of a rotating wind turbine under real operating conditions [5]. In [6], Operational Modal Analysis (OMA) was successfully performed by tracking displacements at 33 target points using stereophotogrammetry combined with strain gauge and LDV data. Nonetheless, these approaches are limited to pre-defined, discrete targets, resulting in relatively low spatial resolution and reduced flexibility during post-processing. Digital Image Correlation (DIC) presents a promising alternative by enabling full-field, three-dimensional displacement measurements across the visible surface of a structure. While DIC is well established for non-rotating systems, its application to rotating machinery remains challenging, since standard DIC algorithms fail when rotational displacements exceed 10°. To overcome this issue, incremental DIC approaches have been developed, wherein the reference image is periodically updated when the measurable angle is exceeded. This method has enabled experimental modal analysis of a rotating tire [7] and disk [8]. However, frequent updates of the reference image introduce cumulative tracking errors. Efforts to reduce these errors have been proposed in [9] and recent research has focused on developing algorithms that improve the accuracy of the initial displacement estimation in DIC. For instance, an efficient 3D DIC initialization algorithm tailored for high rotation angles was proposed in [10], demonstrating robust performance in measuring the displacement of a beam during a three-point bending test. However, while [9] effectively reduces tracking errors, it does not eliminate them entirely, and [10] was validated only on a stationary specimen; thus, its performance under high rotation angles, characteristic of rotor dynamics, has not yet been investigated.

In this paper, a global DIC method is proposed to reconstruct the object rotation during acquisition. The roto-translation parameters are obtained through a Gauss-Newton optimization approach, which minimizes the error at the pixel level. Additionally, to improve computational efficiency, only informative pixels are selected for subsequent elaboration. An experimental validation of the proposed method was obtained by measuring the rotation of a PC fan.

2. Materials and methods

2.1. Hardware setup

A dedicated test bench was arranged to develop and validate the proposed technique. An industrial monochrome camera, Optomotive Smilodon (5120 × 5120 pxl, 1.1”, 150 fps), was equipped with a varifocal lens (Computar 05-VL6Z1626UC-MPYIR) and mounted on a steel plate. A ring light was centered with the optic to provide even illumination of the fan. In front of the camera, a PC fan was mounted on the same plate with a bracket to stand vertically and centered with the camera sensor. The fan has seven blades with a maximum diameter of about 110 mm, and it is powered through a USB cable, allowing for three different rotational speed levels: 1000, 1250 and 1500 rpm. The distance between the fan and the optics was set to obtain a field of view of about 130 × 130 mm^2, so that all the blades of the fan could be acquired by the camera for the whole 360° rotation. Since the fan blades were originally black, the blisk was prepared by spraying a white background, and by adding a black speckle pattern on each blade with a spray can. An overview of the described setup is provided in figure 1.

Figure 1. Developed test bench.

2.2. Tracking algorithm

The main challenge in tracking the motion of rotating structures using conventional DIC algorithms lies in subset rotation. Because traditional DIC algorithms perform the correlation along columns and rows, they struggle to match subsets between frames when rotation occurs. To solve this issue, in this research, the tracking problem is addressed with a global DIC algorithm. Indeed, when a rigid rotation occurs, the displacement of each pixel of the image can be computed through a roto-translation by knowing three scalars, i.e. the rotation angle θ and a 2D translation vector T. It is then possible to relate the reference points' coordinates (X) with the corresponding rotated coordinates (X_r) using the following equation:

$$\begin{aligned} R &= \begin{bmatrix} \cos(\theta) & -\sin(\theta) \\ \sin(\theta) & \cos(\theta) \end{bmatrix} \\ X_\mathrm{r} &= RX + T \end{aligned} \tag{1}$$

Thus, given a sample pixel in the reference image, and assuming that the roto-translation parameters are known, it is possible to compute its coordinates in the rotated image. Additionally, considering that the center of rotation C of the roto-translational does not move during the transformation (i.e. rotated coordinates C_r respect the relation $C_\mathrm{r} = C$), it is possible to relate the translation vector T with the coordinates of center of rotation C.

$$C_\mathrm{r} = RX + T = C \rightarrow T = (I - R)C \tag{2}$$

Given that for general transformations the resulting coordinates will not be integer numbers, it is not possible to directly retrieve the grey level of the rotated point from the rotated image. To overcome this issue, an interpolation scheme (e.g. a bicubic spline interpolation of the image, as presented in [11]) can be adopted to retrieve grey levels at arbitrary locations in the image. Once the grey level at the rotated coordinates (I_q) is known, it is possible to compare its value with the corresponding value of the reference image (I_0), to define a pixel-wise error. This procedure is exemplified in figure 2 for a generic sample point. The described approach assumes knowledge of the roto-translation parameters, which are the unknowns to be found instead. Nevertheless, it is possible to define a list of pixels to be tracked (which do not need to be organized in a regular grid, but can be arbitrary locations in the reference image) and to define an optimization algorithms that finds the best values for θ and T that, applied to the chosen points, minimizes the error between the interpolated transformed image and the reference image.

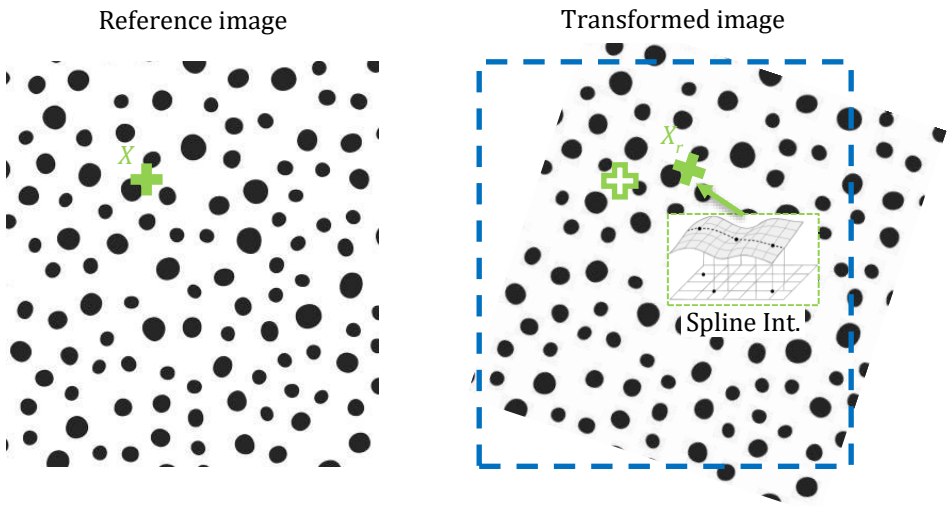

Figure 2. Determination of grey levels after roto-translation.

2.2.1. Gauss-Newton optimization

The described process is non-linear due to the use of the spline interpolation and the trigonometric functions in Eq. 1. Nevertheless, it can be addressed using a Gauss-Newton approach [12,13], which iteratively searches for the minimum of the objective function by taking advantage of the knowledge of the gradients of the function with respect to the optimization variables. In this scenario, the optimization variables are θ and T, while the objective function is defined as the difference between the reference image and the transformed image. The required derivatives can be computed in three stages. First, let $X_{r,1}$ and $X_{r,2}$ represent the horizontal and vertical components of X_r, T_1 and T_2 the horizontal and vertical components of the translation vector T, and R_1 and R_2 the first and second rows of the rotation matrix R, as defined in Eq. 1. The derivatives of the roto-translated coordinates with respect to θ and T can be computed as follows:

$$\begin{aligned}
&\frac{dR_1}{d\theta} = [-\sin(\theta) \quad -\cos(\theta)]; \frac{dR_2}{d\theta} = [\cos(\theta) \quad -\sin(\theta)] \\
&\frac{dX_{r,1}}{d\theta} = \frac{dR_1}{d\theta}X; \frac{dX_{r,2}}{d\theta} = \frac{dR_2}{d\theta}X \\
&\frac{dX_{r,1}}{dT_1} = 1; \frac{dX_{r,1}}{dT_2} = 0; \frac{dX_{r,2}}{dT_1} = 0; \frac{dX_{r,2}}{dT_2} = 1
\end{aligned} \tag{3}$$

Subsequently, given that the grey levels I_q are computed at coordinates X_r, their derivatives with respect to the coordinates can be defined as $dI_q/dX_{r,1}$ and $dI_q/dX_{r,2}$, and computed using Eq. 5 in [11]. Finally, considering that the objective function to be minimized is $E = I_0 - I_q$, and considering that I_0 is a constant, the complete derivatives of E with respect to θ and T can be obtained as:

$$\frac{dI_{\mathrm{q}}}{d\theta} = \frac{dI_{\mathrm{q}}}{dX_{\mathrm{r},1}}\frac{dX_{\mathrm{r},1}}{d\theta} + \frac{dI_{\mathrm{q}}}{dX_{\mathrm{r},2}}\frac{dX_{\mathrm{r},2}}{d\theta}$$
$$\frac{dI_{\mathrm{q}}}{dT_1} = \frac{dI_{\mathrm{q}}}{dX_{\mathrm{r},1}}\frac{dX_{\mathrm{r},1}}{dT_1} + \frac{dI_{\mathrm{q}}}{dX_{\mathrm{r},2}}\frac{dX_{\mathrm{r},2}}{dT_1} \quad (4)$$
$$\frac{dI_{\mathrm{q}}}{dT_2} = \frac{dI_{\mathrm{q}}}{dX_{\mathrm{r},1}}\frac{dX_{\mathrm{r},1}}{dT_2} + \frac{dI_{\mathrm{q}}}{dX_{\mathrm{r},2}}\frac{dX_{\mathrm{r},2}}{dT_2}$$

It is then possible to define an iterative scheme to update the optimization variables and minimize the error:

$$J = \begin{bmatrix} \frac{dI_{\mathrm{q}}}{d\theta} & \frac{dI_{\mathrm{q}}}{dT_1} & \frac{dI_{\mathrm{q}}}{dT_2} \end{bmatrix}; v = \begin{bmatrix} \theta \\ T_1 \\ T_2 \end{bmatrix} \quad (5)$$
$$v_{i+1} = v_i + \left(J^{\mathrm{T}}J\right)^{-1}J^{\mathrm{T}}E$$

Where v, at each iteration stage, contains the updated values of θ and T. The iterations can be stopped when the ratio $\lambda = |v_{i+1} - v_i|/|v_i| < \varepsilon$.

2.2.2. First guess identification

Any iterative optimization algorithm requires a first guess to initialize the optimization, i.e. θ_0 and T_0. In the specific application, the optimization relies on the matching between the speckles in the images. Thus, even if the gradient-based approach outlined in Eq. 5 can direct the optimization along the proper path, it is worth noting that the risk of local minima still exists, especially if the displacement to be tracked is larger than the speckle size (which is often the case for roto-translation). This issue is better clarified in figure 3, where the aforementioned procedure is applied to compute error E, for a given translation and a rotation angle ranging from 0 to 360°. In particular, the value e was plotted for each rotation angle, as defined in the following equation, where n_{p} is the number of elements in E, to represent the average error per pixel (since 8-bit images are used, the values are in the range 0-255):

$$e = \frac{|E|}{\sqrt{n_{\mathrm{p}}}} \quad (6)$$

Additionally, to investigate the effect of a wrong selection of T, which could occur when manually clicking on the image to select the rotation center, a parametric analysis was conducted by moving the rotation center of an increasing radius ρ. The results are shown in figure 3. As can be seen, the error shows seven macroscopic minima along the angular coordinate, in the range of e = 50. This is reasonable since the fan has seven blades; thus, the error has a periodic behaviour. Nevertheless, a sharp minimum corresponding approximately to e_{m} = 12 and θ_{m} = 8.4° can be noted, representing the global optimal rotation angle in the specific case. On the other hand, the curve behaviour along the radial coordinate only shows a global minimum, at least in the investigated range ±100 pxl, which was considered reasonable in the case of manual center selection. To give an insight into the trends around the global minimum, figure 4(a) shows the cross-section of figure 3 with respect to the plane ρ = 0, while figure 4(b) shows the cross-section of the curve with the plane θ = 8.4°. The figure clearly demonstrates a pronounced peak corresponding to the optimal values of the parameters.

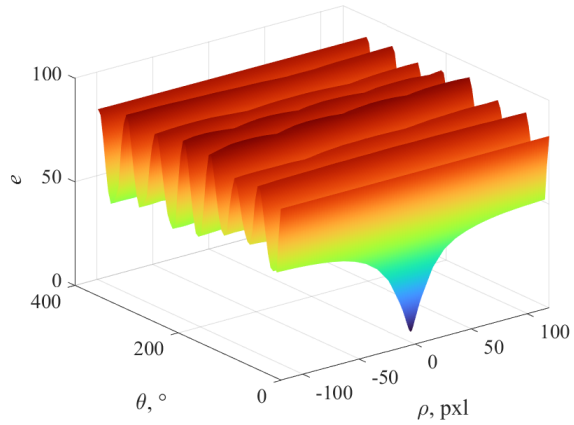

Figure 3. Error between reference and transformed image, for varying angles and translations.

Notably, the peak along the angular coordinate is very sharp, decaying within approximately 0.5°, whereas along the radial coordinate, the peak remains evident over a wider range, approximately ±40 pxl. This indicates that an initial estimate of the center of rotation (T_0) can be manually selected with a relatively large margin of error. Subsequently, the precise value of the angular parameter θ_0 can be determined using a *for-loop* refinement.

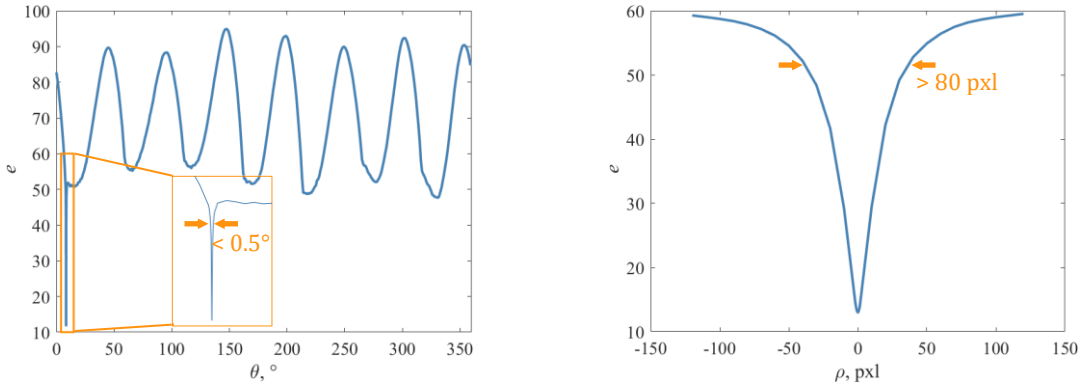

(a) (b)

Figure 4. Intersection of the error surface with: (a) the θ = 8.4° plane and (b) the ρ = 0 plane.

2.2.3. Informative pixel location

Equations 3, 4 and 5 can be applied to all pixels within a given region of interest (ROI), to guide the optimization process and determine the optimal values of θ and T. However, this approach can be computationally inefficient and time-consuming due to the large number of pixels involved. On the other hand, it is worth noting that only the pixels located at the edges of the speckles provide relevant information, since the pixel grey level is highly sensitive to displacement, whereas in uniformly black or white areas, displacements do not result in noticeable changes in grey levels when small displacements occur. To univocally select the informative pixel locations with a robust approach, it is possible to consider the values of the derivative of I_q with respect to the optimization variables (Eq. 4). Those quantities are computed at the pixel level, and the corresponding value can be plotted on the image. In particular, the parameter S_d is considered and defined as follows:

$$S_{\mathrm{d}} = \left(\frac{dI_{\mathrm{q}}}{d\theta}\right)^2 \max\left(\left(\frac{dI_{\mathrm{q}}}{d\theta}\right)^2\right)^{-1} + \left(\frac{dI_{\mathrm{q}}}{dT_1}\right)^2 \max\left(\left(\frac{dI_{\mathrm{q}}}{dT_1}\right)^2\right)^{-1} + \left(\frac{dI_{\mathrm{q}}}{dT_2}\right)^2 \max\left(\left(\frac{dI_{\mathrm{q}}}{dT_2}\right)^2\right)^{-1} \quad (7)$$

Higher values of S_{d} correspond to pixels that are more sensitive to roto-translation and should therefore be prioritized. In this study, all pixels satisfying the condition $S_{\mathrm{d}} > \mathrm{mean}(S_{\mathrm{d}})$ were selected, thus drastically reducing the number of points considered in the analysis. An example of this procedure is shown in figure 5: figure 5(a) displays the S_{d} values for all pixels within the ROI, while figure 5(b) highlights only the selected pixels within the zoomed-in area indicated by the square in figure 5(a).

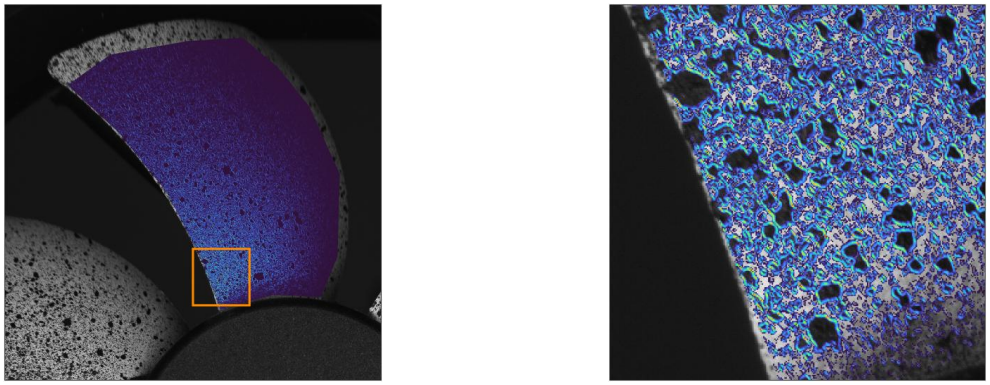

(a) (b)

Figure 5. Selection of informative pixels: (a) value of the parameter S_{d} in the ROI, (b) value of S_{d} for the selected pixels (zoomed view).

The image clearly shows that many pixels of the ROI do not bring relevant information, and would slow down the optimization process without improving the final results. In this particular example, the number of selected pixels is about 25% of the total number of pixels in the ROI, with a consequent significant reduction in computational time.

3. Experimental validation

The proposed algorithm was tested using the simplified setup shown in figure 1. Four images were acquired during the testing, with the first one serving as the reference image. The fan includes a central mark, which facilitates the manual selection of an initial estimate for the center of rotation, and a peripheral mark, which is used to identify the blade number (the closest to the mark was defined as blade 1). The subsequent three images were selected at three different angles with respect to the reference one, approximately at 10°, 45° and 90° respectively, as shown in figure 6(a). The initial estimate of the center of rotation was obtained by manually clicking on the central mark in the image, and this selection was kept constant across all processed images. The initial guess for the rotation angle was determined using the *for-loop* search described in the previous section, using a step size of 0.6°. The iterative optimization process was then initiated, and the results for Image 2 are shown in figure 6(b). The figure is divided into four sub-plots, each displaying a different quantity over the course of the optimization: the rotation angle (θ), the center of rotation (C, having horizontal and vertical coordinates C_{x} and C_{y}, respectively), the average pixel error (e), and the ratio used as the optimization stopping criterion (λ). As can be seen, 85 iterations are needed to complete the optimization.

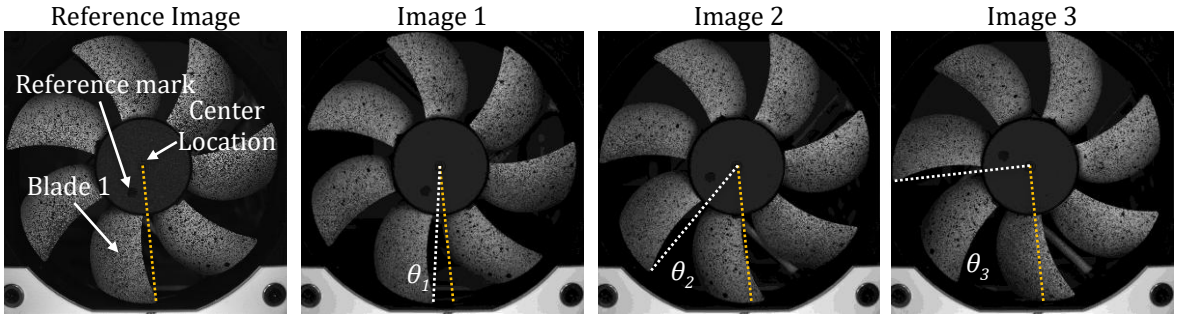

(a)

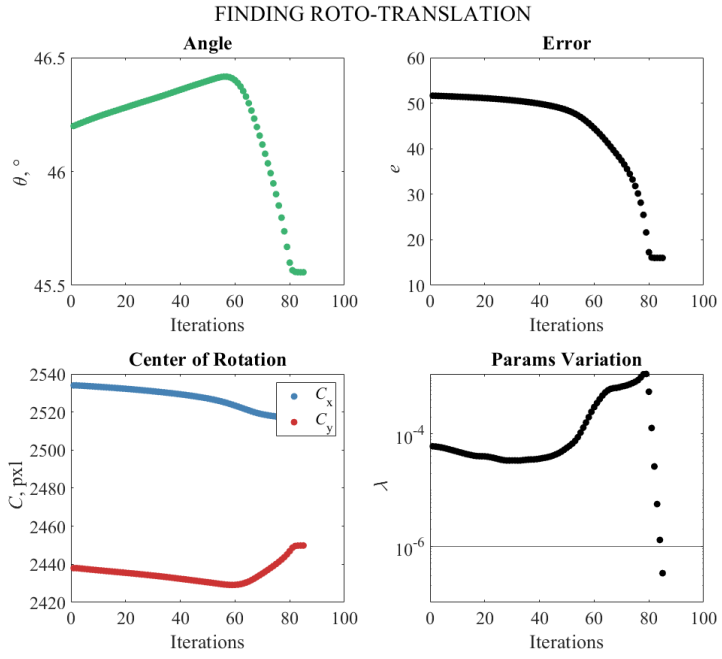

(b)

Figure 6. Experimental data: (a) acquired pictures of the rotating fan and (b) optimization results.

The average error starts with a value of 50 (which is relatively low thanks to the good choice of the first guess through the *for-loop*) and stops with a value of 16, which is comparable to the average measurement error of the pixels, thus demonstrating the success of the optimization process. The total elaboration time for this image was about 3.5 minutes. The optimization was repeated for all the acquired images, and the results are reported in table 1.

Table 1. Outcomes of the optimization process for all the tested images.

Image #	θ_0, °	θ_m, °	C_0, pxl	C_m, pxl	e	Iter. #	Total time, s
1	8.40	8.36		[2515.2; 2451.5]	4.8	6	156
2	46.20	45.62	[2534; 2438]	[2515.5; 2449.9]	16.0	85	209
3	90.60	89.60		[2516.1; 2448.9]	28.9	147	254

The subscript “0” in the table refers to the first guess value, while the subscript “m” refers to the result of the optimization. As can be noted, the final error e increases proportionally with the

rotation angle. This can be ascribed to the fact that, in the case of an angle between the camera optical axis and the fan axes, the blades slightly deform even in the case of rigid body rotation. This phenomenon is more relevant as the rotation angle approaches 90°. Additionally, the optimized location of the center of rotation is not exactly the same for all the images, but lies in the range of a few pixels. Even if it would be possible to rearrange the optimization to impose the same center of rotation for all the images, this was not done because, in principle, the rotor itself can vibrate, thus a different center of rotation can appear in each image. Finally, the optimized parameters were used to compute the roto-translation of all the pixels in the ROI, and to then compute the error $|E|$ in the whole studied region. The results obtained for images 1, 2 and 3 are reported in figure 7(a), (b) and (c), respectively. As can be noted, the error value increases when the angle increases, coherently with the results in table 1.

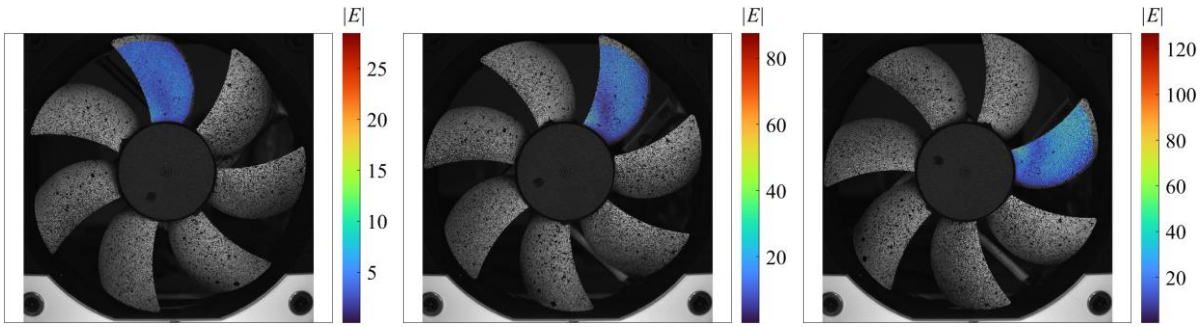

(a) (b) (c)

Figure 7. Error distribution along pixels for: (a) image 1, (b) image 2 and (c) image 3.

4. Conclusion

In this paper, a method to measure rigid body rotation in images is proposed. The approach can be defined as a global digital image correlation (DIC) algorithm, as it optimizes the residuals across all pixels simultaneously using a limited number of optimization variables (i.e., rotation angle and translation) to describe the motion. The algorithm operates by applying a roto-translation to a measurement grid, which can be arbitrarily defined at the pixel level. Grey levels at non-integer coordinates resulting from the roto-translated grid are estimated using a bicubic interpolation scheme. These interpolated values are then compared with the grey levels of the reference image to define an error metric. The optimization process then seeks the roto-translation parameters that minimize this error. Since the derivatives of the interpolation and transformation operations with respect to the optimization variables are known, a Gauss-Newton optimization scheme is used to speed up the process. It was proven that, while the objective function is strongly sensitive to the angle first estimate, it is more compliant in terms of the center of rotation first guess. Thus, the center of rotation is initially manually picked on the image, and the first guess of the rotation angle is retrieved through a *for-loop*. In order to improve computation efficiency, only informative pixels are used for the optimization, i.e. the pixels with higher values of the derivatives of the objective function with respect to the optimization variables.

The proposed approach was evaluated using a dedicated test bench equipped with a camera and a PC fan. Three distinct rotation angles, approximately 10°, 45° and 90°, were selected to assess the algorithm's performance. The identification process was successful for all the tested images, with the resulting error found to be approximately proportional to the actual rotation angle. Future developments will envisage the extension of the method to the measurement of

deformation due to rotation (i.e. image distortion due to non-perfect alignment with the camera) and due to vibrations, to gain a complete insight into the blades' behavior.

References

[1] Boedecker S, Dräbenstedt A, Heller L, Kraft A, Leonhardt A, Pape C, Ristau S, Reithmeier E and Rembe C 2006 Optical derotator for scanning vibrometer measurements on rotating objects *Seventh International Conference on Vibration Measurements by Laser Techniques: Advances and Applications* vol 6345
[2] Lomenzo R O, Barker A J and Wicks A L 2000 Laser vibrometry system for rotating bladed disks *Shock and Vibration Digest* **32**
[3] Zielinski M and Ziller G 2000 Noncontact vibration measurements on compressor rotor blades *Meas Sci Technol* **11**
[4] Battiato G, Firrone C M and Berruti T M 2017 Forced response of rotating bladed disks: Blade Tip-Timing measurements *Mech Syst Signal Process* **85**
[5] Ozbek M, Rixen D J, Erne O and Sanow G 2010 Feasibility of monitoring large wind turbines using photogrammetry *Energy* **35**
[6] Lundstrom T, Baqersad J and Niezrecki C 2013 Using high-speed stereophotogrammetry to collect operating data on a Robinson R44 Helicopter *Conference Proceedings of the Society for Experimental Mechanics Series* vol 6
[7] Minervini D, Mastrodicasa D, Geluk T and Lorenzo E Di 2023 Novel methodology for isolating rotational phenomena in tire testing *INTER-NOISE and NOISE-CON Congress and Conference Proceedings* **268**
[8] Hunady R, Pavelka P and Lengvarsky P 2019 Vibration and modal analysis of a rotating disc using high-speed 3D digital image correlation *Mech Syst Signal Process* **121** 201–14
[9] Occhipinti S, Mastrodicasa D, Manzato S and Di Lorenzo E 2024 Application of digital image correlation in operational modal analysis of rotating structures *ISMA 2024 Conference Proceedings* (Leuven)
[10] Wang Y, Gao Z, Fang Z, Su Y and Zhang Q 2023 Rotating Vibration Measurement Using 3D Digital Image Correlation *Exp Mech* **63**
[11] Neri P, Paoli A, Razionale A V and Barone S 2025 Enhanced subpixel sensitivity in 3D-DIC via Spline-Based correlation map interpolation for vibration measurements *Opt Laser Technol* **188** 112958
[12] Jorge Nocedal and Stephen Wright 2006 *Numerical Optimization (Jorge Nocedal, Stephen Wright)*
[13] Björck Å 1996 *Numerical Methods for Least Squares Problems*